

Carbon Nanostructures as an Electromechanical Bicontinuum

Cristiano Nisoli,¹ Paul E. Lammert,¹ Eric Mockensturm,² and Vincent H. Crespi¹

¹*Department of Physics and Materials Research Institute, The Pennsylvania State University, University Park, Pennsylvania 16802-6300, USA*

²*Department of Mechanical and Nuclear Engineering, The Pennsylvania State University, University Park, Pennsylvania 16802-6300, USA*

(Received 11 April 2007; published 27 July 2007)

A two-field model provides a unifying framework for elasticity, lattice dynamics and electromechanical coupling in graphene and carbon nanotubes, describes optical phonons, nontrivial acoustic branches, strain-induced gap opening, gap-induced phonon softening, doping-induced deformations, and even the hexagonal graphenic Brillouin zone, and thus explains and extends a previously disparate accumulation of analytical and computational results.

DOI: 10.1103/PhysRevLett.99.045501

PACS numbers: 63.22.+m, 62.25.+g, 77.65.-j, 81.05.Tp

Vibrations in carbon nanostructures such as tubes, fullerenes, or graphene sheets [1–3] have a ubiquitous influence on electronic, optical, and thermal response: scattering from optical phonons limits charge transport in otherwise ballistic nanotube conductors [4,5], twist deformations gap metallic tubes [6,7], ballistic phonons transport heat in nanotubes with great efficiency [8–10], resonant Raman spectroscopy can unambiguously identify a tube’s wrapping indices (n, m) [11–14], electron-phonon interactions may ultimately limit the electrical performance of graphene [15,16]. Computationally intensive atomistic models of lattice dynamics often lack simplified model descriptions that can facilitate insight, yet traditional analytical continuum models [1,2,17,18], while very useful and important, cannot describe atomistic phenomena without phenomenological extensions [19–21]. Although continuum models are restricted to long-wavelength physics, they have been used to describe atomic-scale phenomena in bulk binary compounds by incorporating a separate continuum field for each sublattice [22]: in graphene, two fields are necessary. Here we present an analytical “bicontinuum” model that represents the full atomistic detail of the graphenic lattice, including optical modes, nonlinear dispersion of in-plane phonons, electromechanical effects, and even the hexagonal graphenic Brillouin zone, a construct generally held to be exclusively atomistic.

Graphene decomposes into the two triangular sublattices of Fig. 1. We describe in-plane deformations of the sublattices via two fields, $u^i(x)$, $v^i(x)$, $i = 1, 2$, and their strain tensors $u^{ij} = \partial^{(i}u^{j)}$ and $v^{ij} = \partial^{(j}v^{i)}$. The density of elastic energy contains direct and cross terms:

$$V[u, v] = d[u] + d[v] + c[u, v]. \quad (1)$$

Sixfold symmetry of the sublattices implies isotropy of the direct terms [23]:

$$d[u] = \mu' u^{ij} u_{ij} + \frac{\lambda'}{2} u_i^i u_j^j. \quad (2)$$

Symmetry dictates the form of the cross term

$$c[u, v] = 2\mu u^{ij} v_{ij} + \lambda u_i^i v_j^j + \alpha (u - v)^2 - \beta e_{ijk} (u^{ij} + v^{ij})(u^k - v^k). \quad (3)$$

The tensor e_{ijk} , which is invariant under C_{3v} , can be represented by the three unit vectors $\{\hat{e}^{(l)}\}$ of Fig. 1:

$$e_{ijk} = \frac{4}{3} \sum_{l=1}^3 \hat{e}_i^{(l)} \hat{e}_j^{(l)} \hat{e}_k^{(l)}. \quad (4)$$

Only the last term in Eq. (4) is not invariant under general rotation. [In nanotubes, it depends on the helical angle θ_c : $e_{\phi\phi\phi} = -e_{\phi zz} = -\sin(3\theta_c)$, $e_{zzz} = -e_{\phi\phi z} = -\cos(3\theta_c)$, where ϕ, z are defined in Fig. 1.] This elastic energy density, the lowest-order approximation in both derivatives and fields, contains six parameters: μ' and λ' , being confined to one sublattice, describe next-neighbor interactions; the cross terms μ and λ describe nearest-neighbor interaction; α describes the stiffness against relative shifts of the sublattices; β determines the strength of rotational symmetry breaking and so carries the point group symmetry of graphene. These parameters are normalized to the sublattice surface density σ_s , so that the elastic energy is $W = \int \sigma_s V d^2x$.

Taking $\frac{1}{2} \sigma_s (\dot{u}^2 + \dot{v}^2)$ as the surface density of kinetic energy, the equations of motion read

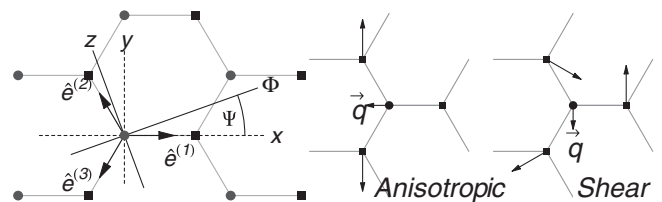


FIG. 1. The two sublattices (circles and squares) of graphene and the three unit vectors $\hat{e}^{(l)}$ used in the text. ϕ, z are cylindrical coordinates of a tube, while $\Psi = \pi/6 - \theta_c$ with θ_c the chiral angle. Also, anisotropic ($u^{xx} = u^{xy} = 0$, $u^{yy} = 2\gamma$, $q^x = \ell\gamma$), shear ($u^{xx} = u^{yy} = 0$, $u^{xy} = \eta$, $q^y = -\ell\eta$) strains.

$$\begin{aligned}\ddot{u}^i &= \partial_j \sigma_{(u)}^{ij} - 2\alpha(u^i - v^i) + \beta e_{lm}^i (v^{lm} + u^{lm}), \\ \ddot{v}^i &= \partial_j \sigma_{(v)}^{ij} + 2\alpha(u^i - v^i) - \beta e_{lm}^i (v^{lm} + u^{lm}),\end{aligned}\quad (5)$$

with the sublattice 2D stress tensors

$$\begin{aligned}\sigma_{(u)}^{ij} &= 2\mu' u^{ij} + \lambda' \delta^{ij} u_k^k + 2\mu v^{ij} + \lambda \delta^{ij} v_k^k - \beta e_k^{ij} (u^k - v^k), \\ \sigma_{(v)}^{ij} &= 2\mu' v^{ij} + \lambda' \delta^{ij} v_k^k + 2\mu u^{ij} + \lambda \delta^{ij} u_k^k - \beta e_k^{ij} (u^k - v^k).\end{aligned}\quad (6)$$

As expected, α determines the frequency of two degenerate $k = 0$ optical modes: $\omega_\Gamma^2 = 4\alpha$.

First, we briefly show that the usual macroscopic elastic energy of graphene and its Lamé coefficients can be obtained from V . A static, uniform solution of Eqs. (5) returns identical deformations on both lattices with an internal displacement $2q^i \equiv u^i - v^i$:

$$2q^i = \ell e_{lm}^i u^{lm} = \ell e_{lm}^i v^{lm}, \quad (7)$$

where $\ell = \beta/\alpha$ is a characteristic length. Anisotropic ($2\gamma = u^{xx} - v^{yy}$) and shear ($\eta = u^{xy}$) strains produce internal displacements $q^x = \ell\gamma$ and $q^y = -\ell\eta$ (Fig. 1). The elastic energy for uniform deformations $W_u = \int V_u \sigma_g d^2x$ then simplifies to

$$\begin{aligned}V_u[u, q] &= \left(\mu_R + \frac{\beta^2}{\alpha}\right) u^{ij} u_{ij} + \frac{1}{2} \left(\lambda_R - \frac{\beta^2}{\alpha}\right) u_i^i u_j^j \\ &\quad + 2\alpha q^2 - 2\beta e_{ijk} u^{ij} q^k,\end{aligned}\quad (8)$$

where $\sigma_g = 2\sigma_s$ is the surface density of graphene, $\mu_R \equiv \mu + \mu' - \beta^2/\alpha$, $\lambda_R \equiv \lambda + \lambda' + \beta^2/\alpha$ the measurable Lamé coefficients [23]. Macroscopic problems do not distinguish between the two sublattices; eliminating q^i in Eq. (8) through Eqs. (4) and (7) we obtain the familiar, isotropic, macroscopic energy for graphene, $V_u = \mu_R u^{ij} u_{ij} + \lambda_R u_i^i u_j^j/2$. In the long-wavelength limit Eqs. (5) return the familiar longitudinal and transverse speeds of sound in terms of the Lamé coefficients: $v_L^2 = 2\mu_R + \lambda_R$, $v_T^2 = \mu_R$.

The out-of-plane displacements $u_\perp(x)$ and $v_\perp(x)$ do not couple with the in-plane u^i, v^i in the harmonic limit: invariance under simultaneous sign change of u_\perp and v_\perp prevents it, for flat sheets. Introducing $2p_\perp(x) = u_\perp(x) + v_\perp(x)$ and $2q_\perp(x) = u_\perp(x) - v_\perp(x)$, V_\perp must be invariant under $p_\perp \rightarrow p_\perp + L(x)$, $L(x)$ a linear function in the plane, and thus, can contain only second (and higher) derivatives in p_\perp . Symmetry dictates (cf. the appendix)

$$\begin{aligned}V_\perp &= 4\alpha_\perp q_\perp^2 - 4\alpha'_\perp \partial_i q_\perp \partial^i q_\perp + 4\beta_\perp e_{ijk} \partial^k q_\perp \partial^{ij} p_\perp \\ &\quad + 2\mu_\perp^+ \partial_{ij} p_\perp \partial^{ij} p_\perp + \lambda_\perp^+ \partial_i p_\perp \partial^i p_\perp \\ &\quad - 2\mu_\perp^- \partial_{ij} q_\perp \partial^{ij} q_\perp - \lambda_\perp^- \partial_i q_\perp \partial^i q_\perp.\end{aligned}\quad (9)$$

The frequency of the $k = 0$ out-of-plane optical mode is $2\sqrt{\alpha_\perp}$, and the out-of-plane acoustic branch is quadratic at small wave vector, as expected.

The bicontinuum phonons are much more richly structured than in a traditional continuum model: they include all the optical branches, show nonlinear dispersion at large wave vector, and even display the main features of the Brillouin zone, all without sacrificing the advantages of a continuum framework. Plane-wave solutions of Eqs. (5) return an analytically solvable fourth-order secular equation in $\omega(k)$, yielding two acoustic and two optical branches. The longitudinal branches cross at the vertices of a hexagon. Since the two-field elastic energy density respects the point group symmetry of the graphene lattice, this hexagon is oriented just as the graphene Brillouin zone; although the model, unlike in the envelope function approach [24], has no built-in length scale, the elastic parameters can be constrained so that the crossing point coincides with the K point of graphene. A similar argument holds for the out-of-plane modes [25]: strikingly *one can construct the correct Brillouin zone within a continuum model*. Figure 2 shows the bicontinuum phonons fit to electron-energy-loss spectroscopy data [26,27] for parameters fitted either to the full Brillouin zone or just around Γ [28].

The bicontinuum provides a unified framework for nanotube mechanics which can describe *all* current computational results on the coupling of nanotube phonons to static structural distortions to each other (e.g., breathing-to-Raman or longitudinal-to-transverse modes in helical

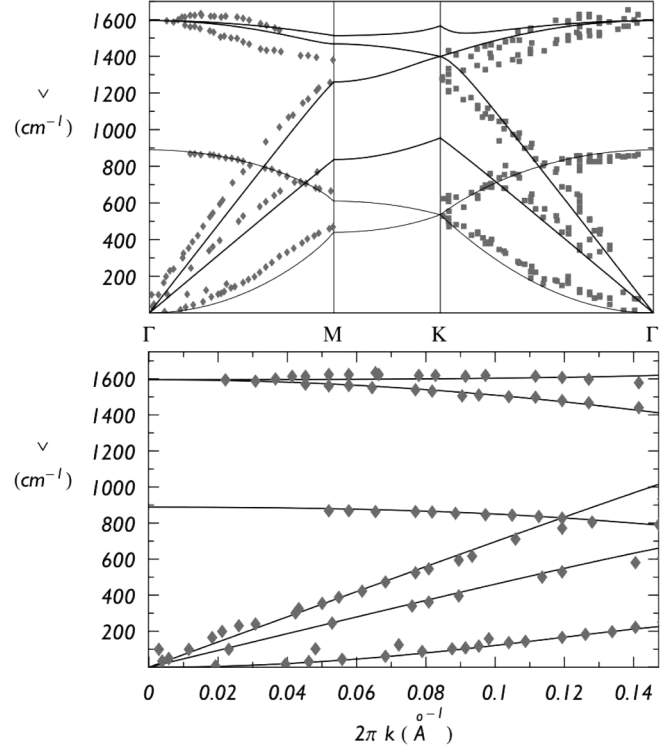


FIG. 2. Bicontinuum phonons compared to electron-energy-loss spectroscopy data (diamonds [26] and squares [27]), fitting either to the entire Brillouin zone (top) or just around Γ along $\Gamma \rightarrow M$.

tubes) and to the tube electronic structure. In a cylindrical geometry with coordinates $\{r, \phi, z\}$, a coupling between the tangential displacements u^i , and the radial $u^r = u_\perp$ appears in V of Eq. (1) via $u^{\phi\phi} = (\partial_\phi u^\phi + u^r)/r$ (and similarly for v); this accounts for the emergence of the radial breathing mode (RBM) [29]. We consider uniform solutions: $u = u_o e^{-i\omega t}$, $v = v_o e^{-i\omega t}$. The tube's helicity can be subsumed into new axes $\{\xi, \zeta\}$ ($\xi = \phi \cos 3\theta_c + z \sin 3\theta_c$, $\zeta = -\phi \sin 3\theta_c + z \cos 3\theta_c$) rotated by an angle $3\theta_c$ with respect to the base of the tube. In terms of p, q we obtain $p^\xi, p^\zeta = 0$ and

$$\begin{aligned} q^\zeta(\omega^2 - 4\alpha) + 2\frac{\beta}{r}p^r &= 0 \\ p^r\left(\omega^2 - \frac{v_L^2 + \beta^2/\alpha}{r^2}\right) + 2\frac{\beta}{r}q^\zeta &= 0 \\ q^\xi(\omega^2 - 4\alpha) &= 0 \\ q^r\left(\omega^2 - 4\alpha_\perp + \frac{2\mu - 2\mu' + \lambda - \lambda'}{r^2}\right) &= 0. \end{aligned} \quad (10)$$

Unlike standard elasticity [17], which cannot describe optical modes, or standard atomistic descriptions, which cannot be solved analytically, the two-field continuum model enables an exact analytical solution for the coupling between the RBM and the graphitelike optical mode through the first two equations in (10); the RBM induces a shear in the sublattices, $u^{\phi\phi} = v^{\phi\phi} = u^r/r$, which couples with the internal displacement through β , and vice versa. Thus, the RBM is not purely radial, but has a longitudinal component $q_B^z \sim (\ell/2r) \cos 3\theta_c$, as previously seen in a numerical calculation [30]. Expansion of the RBM frequency in powers of ℓ/r reveals a correction to the standard continuum result v_L/r [17]: $\omega_B = (v_L/r) \times [1 - \frac{1}{8}(\frac{\ell}{r})^2 + O(\frac{\ell}{r})^4]$. The graphitelike optical modes of chiral tubes are $\omega_\xi = \sqrt{4\alpha}$, $\omega_\zeta/\omega_\xi = 1 + \frac{1}{8}(\frac{\ell}{r})^2 + O(\frac{\ell}{r})^4$, also of mixed longitudinal/transverse character except for armchair and zigzag nanotubes, while the out-of-plane optical mode $\omega_\perp = [4\alpha_\perp - (2\mu - 2\mu' + \lambda - \lambda'/r^2)]^{1/2}$ is purely radial. A density functional theory calculation of the breathing mode [31] reports different frequencies with (ω_B) and without ($\tilde{\omega}_B$) coupling to optical modes. We predict $r^2(\tilde{\omega}_B^2 - \omega_B^2) \rightarrow \beta^2/\alpha$ as $r \rightarrow \infty$: using Ref. [31] data for $\tilde{\omega}_B, \omega_B$ we obtain $\ell \equiv \beta/\alpha = 0.25 \text{ \AA}$ (0.27 \AA) for nonmetallic zigzag (armchair) tubes, in good agreement with the parameters from our fit to the graphene phonons [28].

The bicontinuum can also describe electron-lattice coupling to both acoustic and optical modes, by incorporating a tight-binding model whose nearest-neighbor hopping integrals $t^{(1)}, t^{(2)}, t^{(3)}$ are modulated by the in-plane elastic deformations:

$$dt^{(l)} = -\tau \hat{e}_i^{(l)} \hat{e}_j^{(l)} u^{ij} + \tau \hat{e}_i^{(l)} q^i/e, \quad (11)$$

where e is the interatomic distance and τ a parameter to be determined [32]. For example, lattice deformations open

gaps in metallic tubes, and these gaps in turn affect vibrational frequencies. If ϵ_c, ϵ_v are the conduction and valence bands, we have to nearest neighbors

$$\epsilon_c(k)^2 - \epsilon_v(k)^2 = \sum_l t^{(l)} + 2 \sum_{m>l} t^{(l)} t^{(m)} \cos(ka^{(m)}), \quad (12)$$

where $a^{(n)} \equiv e^{(l)} - e^{(m)}$, $n(l, m)$ is cyclic in $\{1, 2, 3\}$ (e.g., $a^{(3)} \equiv e^{(1)} - e^{(2)}$) and $\{e^{(i)}\}$ connects nearest neighbors. From Eqs. (11) and (12) we find the band gap opened by strain in a metallic nanotube to be

$$\begin{aligned} \frac{\Delta^2}{(3\tau)^2} &= \frac{1}{2} u^{ij} u_{ij} - \frac{1}{4} u_i^i u_i^i - \frac{1}{e} e_{ijk} u^{ij} q^k + \frac{1}{e^2} (\hat{z}_i q^i)^2 \\ &+ \frac{1}{e} e_{ijk} \hat{\phi}^k u^{ij} \hat{\phi}_h q^h - \frac{1}{4} (e_{ijk} u^{ij} \hat{\phi}^k)^2. \end{aligned} \quad (13)$$

In the second line of Eq. (13) the symmetry of the honeycomb lattice is broken by the unit vectors $\hat{\phi}^i, \hat{z}^i$ of the cylindrical coordinates. In terms of $2\gamma' \equiv u^{\phi\phi} - u^{zz}$, $\eta' \equiv u^{\phi z}, q^z$, Eq. (13) reads

$$\Delta = 3\tau |q^z/e + \gamma' \cos(3\theta_c) + \eta' \sin(3\theta_c)|, \quad (14)$$

which corrects and extends a well-known previous result within a one-field continuum model [7] that neglected the inner displacement (i.e., $q^i = 0$).

Opening band gaps in metallic nanotubes causes several shifts in observed quantities. The term proportional to q_z^2 in Eq. (13) shows that longitudinal optical modes open a band gap in metallic tubes of any helicity; the elastic energy lowers by a term proportional to the square of the band gap, leading to a softening of longitudinal optical frequency in metallic nanotubes, as revealed by a recent density-functional theory (DFT) study [33]. Equation (13) predicts also a softening of the RBM in metallic nanotubes $\delta\omega_B/\omega_B = -A \cos^2(3\theta_c)$, highest for zigzag tubes as seen in DFT [31], and relates it to the optical softening, with $A = (1 - \ell/e) \omega_{\text{opt}} \delta\omega_{\text{opt}} e^2 / 4v_L^2$, ω_{opt} the graphitelike optical mode, and $\delta\omega_{\text{opt}}$ its softening in metallic tubes ($A \approx 2\%$). Other shifts can be predicted: the speed of sound for the twist mode softens by $\Delta c_t/c_t = -(v_L^2/2v_T^2) A \sin^2(3\theta_c)$, or $\approx 2.2\%$ in armchair tubes.

Doping-induced structural deformations can also be studied by minimizing the total energy (elastic plus doped electrons). Subtle phenomena absent in other models [34] can be accessed within the bicontinuum framework. Going to next-nearest neighbor in the hopping integrals ($dt_1^{(l)} = -\tau_1 \hat{a}_i^{(l)} \hat{a}_j^{(l)} v^{ij}$ [32]), we find that at first order in both a/r and the number of dopant electrons per atom ρ_e , semi-conducting $(n, 0)$ nanotubes show doping-induced changes in tube length ($dL/L = u^{zz}$) and axial bond length ($db_{\text{ax}} = eu^{zz} - q^z$):

$$\begin{aligned} dL/L &= \frac{\rho_e \tau}{8m_C v_T^2} \left[\pm \left(1 - \frac{\ell}{e}\right) + \frac{3\tau_1}{2\tau} \frac{2\mu_R + \lambda_R}{\mu_R + \lambda_R} \right], \\ db_{\text{ax}} &= \pm \frac{\rho_e \tau}{2m_C \omega_{\text{opt}}^2 e}, \end{aligned} \quad (15)$$

where m_C is the mass of the carbon atom. The sign is positive (negative) for $r = n$ and $3 = 1$ ($n \bmod 3 = 1$). Recent DFT results [35] indeed show shrinking or stretching of b_{ax} for $n = 16, 13$ or $n = 14, 11$ tubes, respectively, as predicted by Eq. (15). In DFT, the overall tube lengthens in the second case ($n = 14, 11$), again in accord with the bicontinuum; the lengthening found for $r = 2$ is less than for $r = 1$, perhaps a consequence of the change in sign in Eq. (15). Finally the shrinking of the axial bond determines an upshift in the longitudinal graphitelike optical mode and might explain recent Raman results that point toward anomalous bond contraction under doping in semiconducting nanotubes [36,37].

A full range of vibrational-electronic-mechanical couplings, which were absent from previous continuum models or happened upon in an *ad hoc* fashion in computational work, can now be understood within a single unified analytical framework. Extending the formalism to include higher-order effects arising from curvature or metallic character [i.e., symmetry breaking terms containing $\hat{\phi}^i$, \hat{z}^i , as in Eq. (13)], anharmonicity (terms higher order in u^{ij} , v^{ij}), or long-distance interactions (higher partial derivatives) is straightforward. An extension to boron nitride nanotubes, with different coefficients for each sublattice in the direct terms of Eq. (2), might prove useful to study their piezoelectricity.

Appendix: Derivation of Eq. (3).—The term $c[u, v]$ must be invariant under the combination of $2\pi/6$ rotations and the exchange of fields $u \leftrightarrow v$. Adding reflection through the x axis (Fig. 1) then implies C_{3v} invariance. There is also a field translation invariance: $u(x) \rightarrow u(x) + p$, $v(x) \rightarrow v(x) + p$. The objects u^i , v^j , u^{ij} , and v^{ij} can be combined pairwise only into tensors of rank two, three, and four; thus $c[u, v]$ decomposes into three parts. The first part has terms like $u^i v^j$; symmetry then implies the form $\alpha(u - v)^2$ with $\alpha > 0$ to ensure an energy minimum. The second part has terms like $u^{ij} v^{kl}$; the only admissible form is $2\mu u^{ij} v_{ij} + \lambda u_i^i v_j^j$. The third part contains only rank three terms such as $u^{ij} v^k$ contracted with a C_{3v} invariant tensor e_{ijk} , giving $e_{ijk} u^{ij} v^k$. By requiring invariance under $2\pi/6$ rotations conjugated with sublattice switching, and also the field translation invariance, we obtain the form $e_{ijk} u^{ij} (u^k - v^k) + e_{ijk}^* v^{ij} (v^k - u^k)$, where the star means a $2\pi/6$ rotation. Since C_{3v} invariance implies $e_{ijk}^* = -e_{ijk}$ we finally obtain the third row of Eq. (3).

-
- [1] S. Iijima, *Nature (London)* **354**, 56 (1991).
 [2] R. Saito, G. Dresselhaus, and M. S. Dresselhaus, *Physical Properties of Carbon Nanotubes* (Imperial College Press, London, 1998).
 [3] M. S. Dresselhaus, G. Dresselhaus, and P. C. Eklund, *Science of Fullerenes and Carbon Nanotubes* (Academic, New York, 1996).
 [4] S. J. Tans *et al.*, *Nature (London)* **386**, 474 (1997).

- [5] C. L. Kane *et al.*, *Europhys. Lett.* **41**, 683 (1998).
 [6] A. Rochefort, P. Avouris, F. Lesage, and D. R. Salahub, *Phys. Rev. B* **60**, 13 824 (1999).
 [7] L. Yang and J. Han, *Phys. Rev. Lett.* **85**, 154 (2000).
 [8] S. Berber, Y.-K. Kwon, and D. Tománek, *Phys. Rev. Lett.* **84**, 4613 (2000).
 [9] H.-Y. Chiu *et al.*, *Phys. Rev. Lett.* **95**, 226101 (2005).
 [10] P. Kim, L. Shi, A. Majumdar, and P. L. McEuen *Phys. Rev. Lett.* **87**, 215502 (2001).
 [11] E. Richter and K. R. Subbaswamy *Phys. Rev. Lett.* **79**, 2738 (1997).
 [12] R. Saito *et al.*, *Phys. Rev. B* **64**, 085312 (2001).
 [13] A. Jorio *et al.*, *Phys. Rev. Lett.* **86**, 1118 (2001).
 [14] A. Jorio, R. Saito, G. Dresselhaus, and M. S. Dresselhaus, *Phil. Trans. R. Soc. A* **362**, 2311 (2004).
 [15] K. S. Novoselov *et al.*, *Nature (London)* **438**, 197 (2005).
 [16] S. Y. Zhou *et al.*, *Nature Phys.* **2**, 595 (2006).
 [17] G. D. Mahan, *Phys. Rev. B* **65**, 235402 (2002).
 [18] H. Suzuura and T. Ando, *Phys. Rev. B* **65**, 235412 (2002); A. Raichura *et al.*, *J. Appl. Phys.* **94**, 4060 (2003); S. V. Goupalov, *Phys. Rev. B* **71**, 085420 (2005).
 [19] F. Comas *et al.*, *Phys. Rev. B* **47**, 7602 (1993).
 [20] L. Chico and R. Pérez-Álvarez *Phys. Rev. B* **69**, 035419 (2004); **73**, 075425 (2006).
 [21] Y. N. Gartstein *et al.*, *Phys. Rev. B* **68**, 115415 (2003).
 [22] H. Deresiewicz *et al.*, *The Collected Papers of Raymond D. Mindlin* (Springer-Verlag, New York, 1989).
 [23] L. D. Landau and E. M. Lifshitz, *Theory of Elasticity* (Pergamon Press, Oxford, 1986). The density of elastic energy for an isotropic system has the form $f = \mu u^{ij} u_{ij} + \frac{\lambda}{2} u_i^i u_j^j$, where λ , μ are the Lamé coefficients. Here we renormalize the coefficients to $\sigma_g = 1$.
 [24] B. A. Foreman, *Phys. Rev. B* **52**, 12260 (1995).
 [25] See EPAPS Document No. E-PRLTAO-99-048730 for derivation of out-of-plane spectrum. For more information on EPAPS, see <http://www.aip.org/pubservs/epaps.html>.
 [26] C. Oshima *et al.*, *Solid State Commun.* **65**, 1601 (1988).
 [27] S. Siebentritt, R. Pues, K. H. Rieder, and A. M. Shikin, *Phys. Rev. B* **55**, 7927 (1997).
 [28] The fit around Γ returns (in Kms^{-1}) $v_L = 21$, $v_T = 14$, $(-2\mu + 2\mu' - \lambda + \lambda' + \beta^2/\alpha)^{1/2} = 4.4$, $(\mu - \mu')^{1/2} = 15.6$, and $\ell \equiv \beta/\alpha = 0.3 \text{ \AA}$. The fit to the full zone uses $v_L = 16.5$, $v_T = 10.8$, $(2\mu - 2\mu' + \lambda - \lambda' - \beta^2/\alpha)^{1/2} = 8.7$, $(\mu - \mu')^{1/2} = 6.6$, $\ell = 0.24 \text{ \AA}$; an extension to higher derivatives would improve the agreement.
 [29] Wrapping graphene into a tube breaks the hexagonal symmetry and introduces new terms in V as curvature corrections, which for simplicity we will not consider here.
 [30] E. Dobardžić *et al.*, *Phys. Rev. B* **68**, 045408 (2003).
 [31] J. Kürti *et al.*, *New J. Phys.* **5**, 125 (2003).
 [32] $t^{(l)}$, $t_1^{(l)}$ are the absolute values of the hopping integrals for nearest and next-nearest neighbors. We assume they depend only on distance: $dt = -\tau de/e$, $dt_1 = -\tau_1 da/a$.
 [33] O. Dubay *et al.*, *Phys. Rev. Lett.* **88**, 235506 (2002).
 [34] M. Verissimo-Alves, B. Koiller, H. Chacham, and R. B. Capaz, *Phys. Rev. B* **67**, 161401(R) (2003).
 [35] R. E. Margine *et al.* (to be published).
 [36] G. Chen *et al.* *Phys. Rev. B* **72**, 155406 (2005).
 [37] G. Chen *et al.*, *Phys. Rev. B* **71**, 045408 (2005).